Electronic Supplementary Material (ESI) for Physical Chemistry Chemical Physics.

Supporting Information

Inverse Design of Molecule−Metal Nanoparticle Systems Interacting with Light for Desired Photophysical Properties

Takafumi Shiraogawa,*[a] Giulia Dall'Osto,[b] Roberto Cammi,[c] Masahiro Ehara,*[a, d, e] Stefano Corni*[b, f]

[a]SOKENDAI, The Graduate University for Advanced Studies, 38 Nishigonaka, Myodaiji, Okazaki, 444-8585, Japan.

[b]Department of Chemical Sciences, University of Padova, via Marzolo 1, Padova, Italy.

[c]Department of Chemical Science, Life Science and Environmental Sustainability, University of Parma, Parma, Italy.

[d]Institute for Molecular Science and Research Center for Computational Science, 38 Nishigonaka, Myodaiji, Okazaki, 444-8585, Japan.

[e]Elements Strategy Initiative for Catalysts and Batteries (ESICB), Kyoto University, Kyoto, 615-8245, Japan.

[f]CNR Institute of Nanoscience, via Campi 213/A, Modena, Italy.

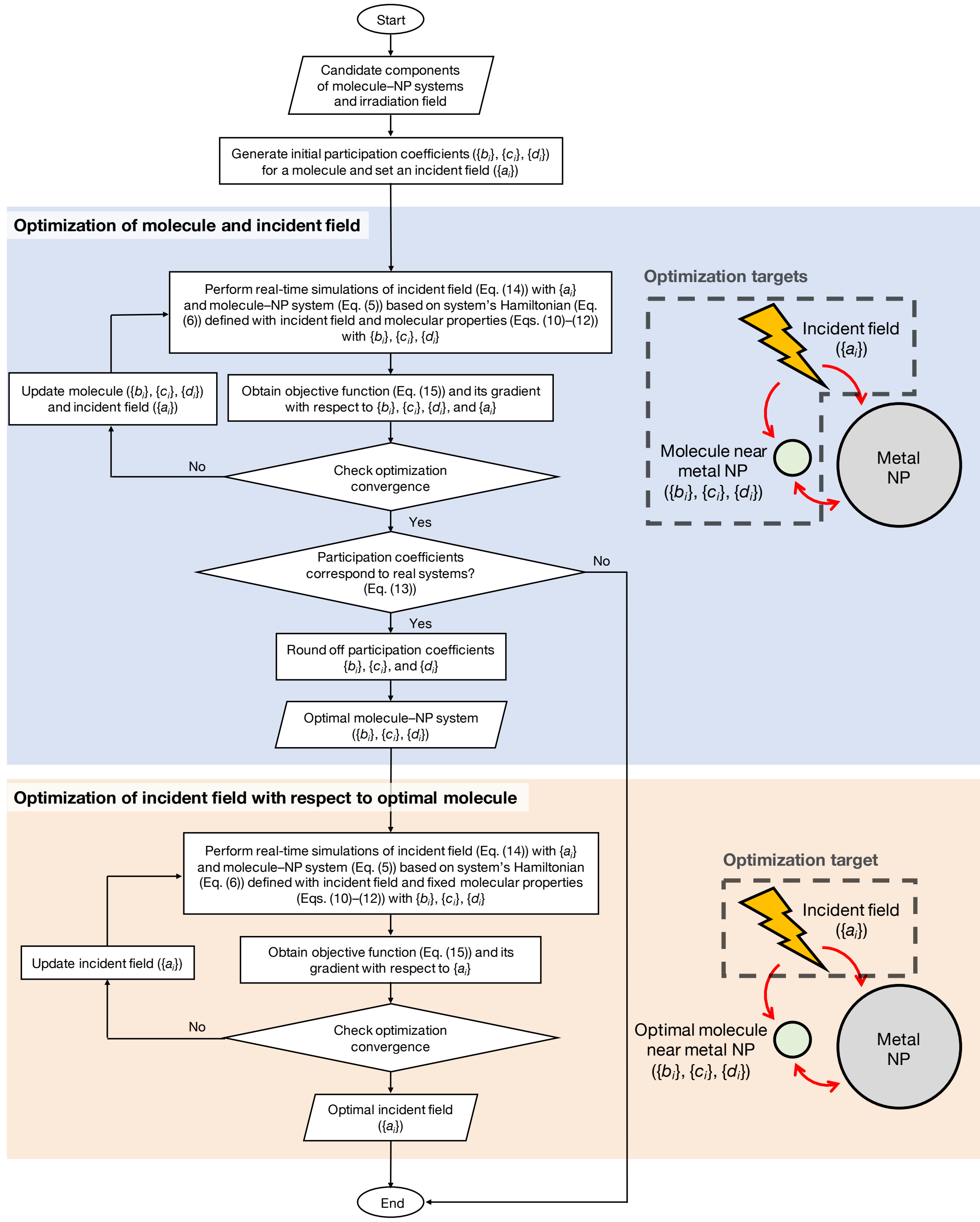

Scheme S1. Simplified flowchart of inverse design of molecule–NP system and incident field.

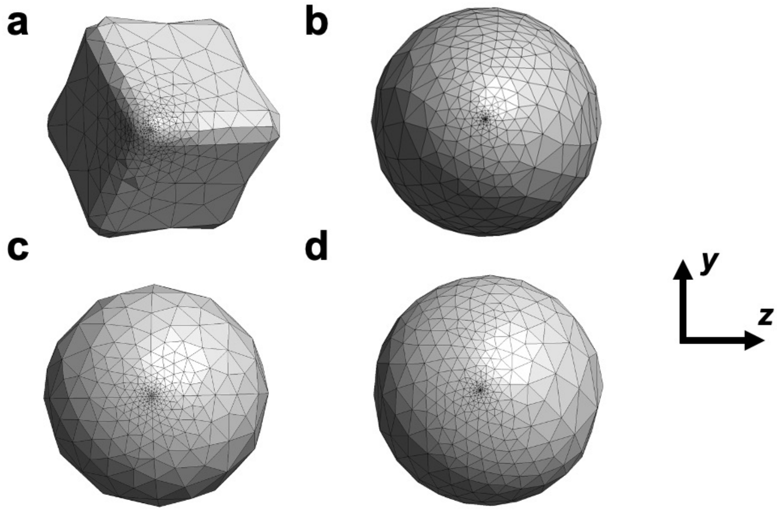

Figure S1. Candidate metal NPs of (a) cubic, (b) ellipsoidal, (c) rod, and (d) spherical shapes. The view from the *x* axis.

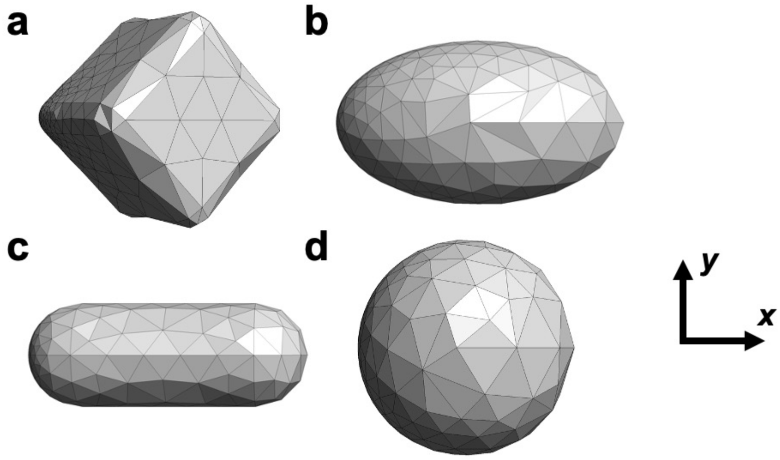

Figure S2. Candidate metal NPs of (a) cubic, (b) ellipsoidal, (c) rod, and (d) spherical shapes. The view from the *z* axis.

For Figures S3 and S4, we have performed calculations in the time domain using a time step of 0.1 a.u. (2.42 as) with a propagation time of 3400 a.u. (82.24 fs) when the system is interacting with a narrow Gaussian electric field polarized along the x direction, with pulse width 4 a.u. (96.8 as), centered at 20 a.u. (0.48 fs) and with amplitude of 10^{-6} a.u. The spectra are obtained as the Fourier transform of the NP dipole propagation.

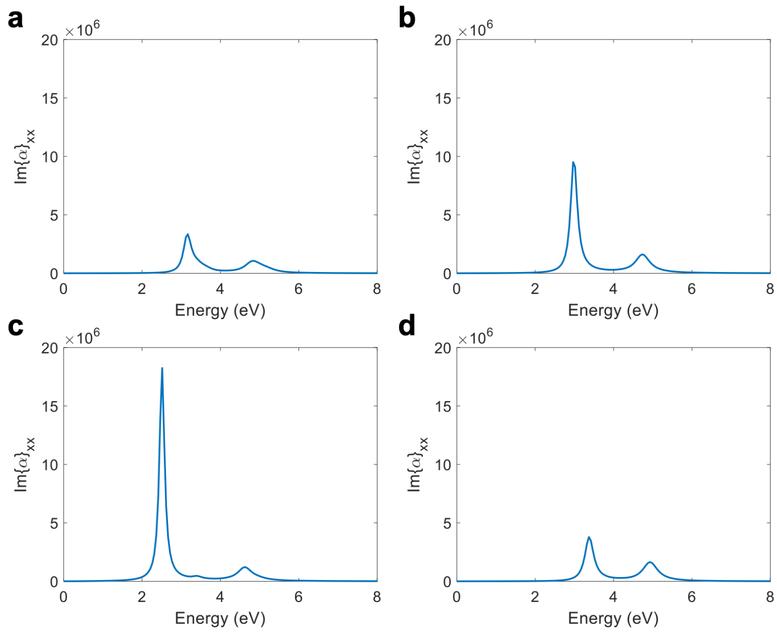

Figure S3. Imaginary part of the polarizability of the silver NPs with (a) cubic, (b) ellipsoidal, (c) rod, and (d) spherical shapes.

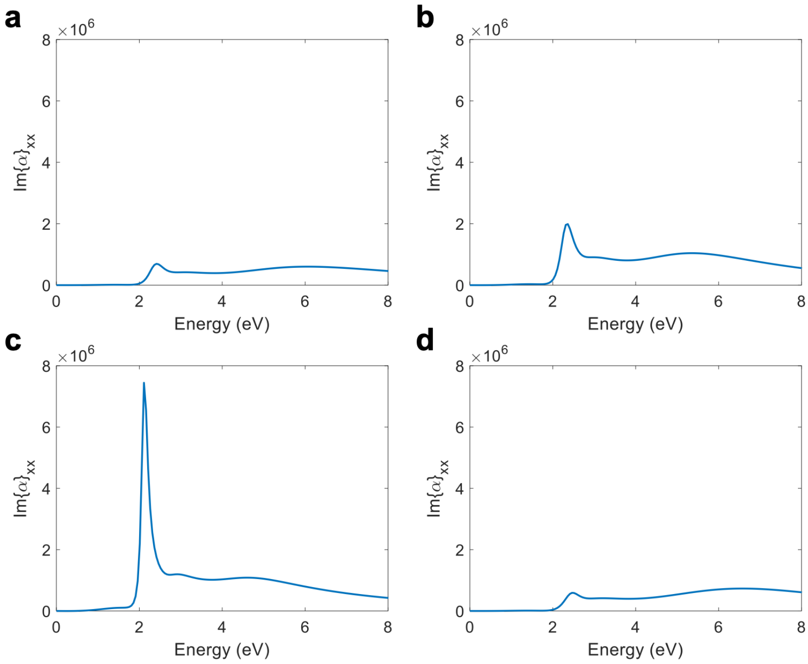

Figure S4. Imaginary part of the polarizability of the gold NPs with (a) cubic, (b) ellipsoidal, (c) rod, and (d) spherical shapes.

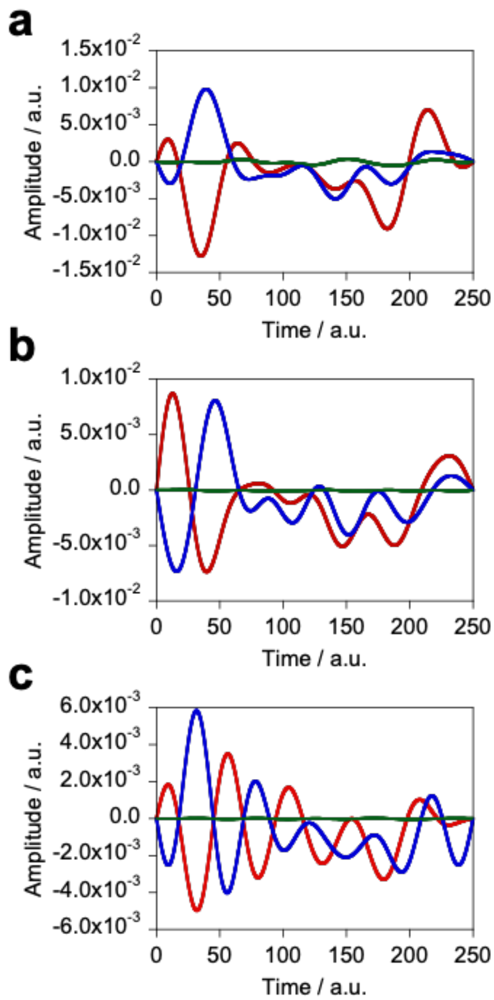

Figure S5. Time profiles of the optimal incident fields designed with the penalty factor α of (a) 1, (b) 10, or (c) 100 a.u. for the field fluence. The red, blue, and green lines are the x, y, and z components, respectively.

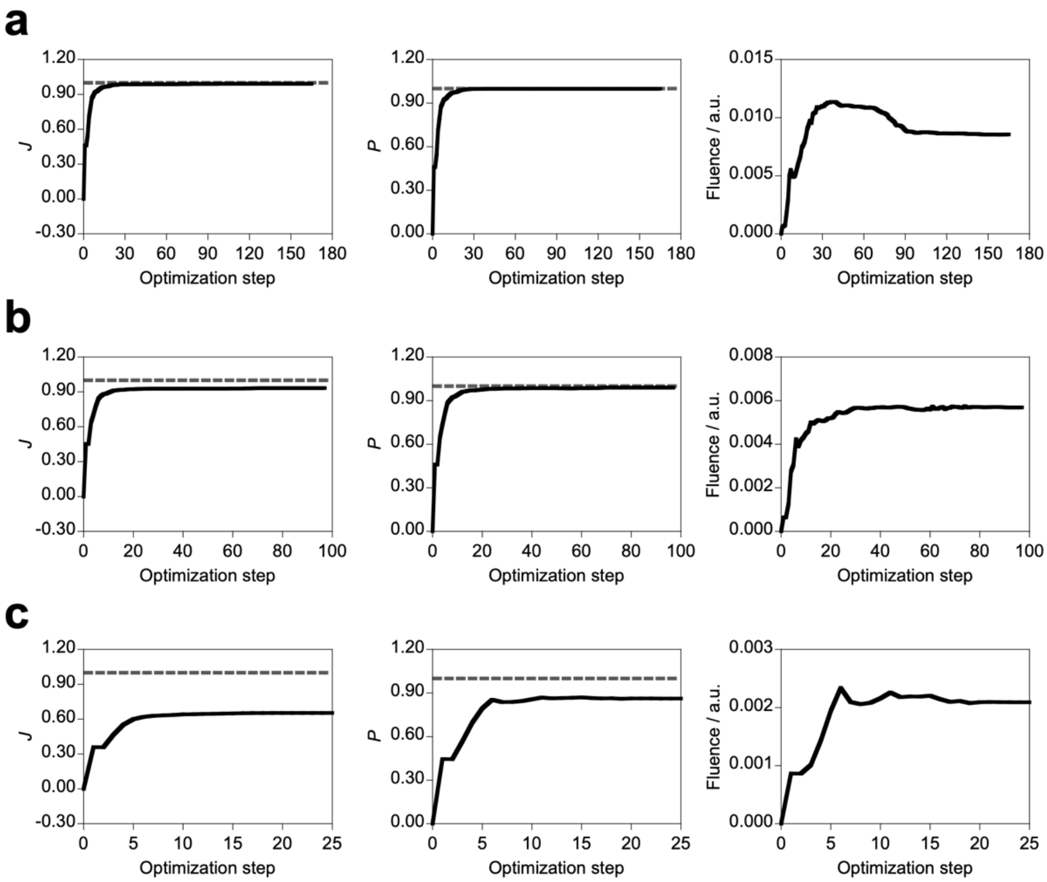

Figure S6. Optimization histories of the objective function in the design of the optimal incident field with the different penalty factors α of (a) 1, (b) 10, and (c) 100 a.u. for the field fluence, along with variations of population of the target state and total fluence of the incident field. The gray dashed lines denote the value of 1.00.

Table S1. Penalty factor γ used in the design of both the molecule and incident field on the various metal NPs

NP shape	Metal nature	
	Ag	Au
Cube	1.05	1.05
Ellipsoid	1.05	-
Rod	1.20	1.05
Sphere	1.20	1.20

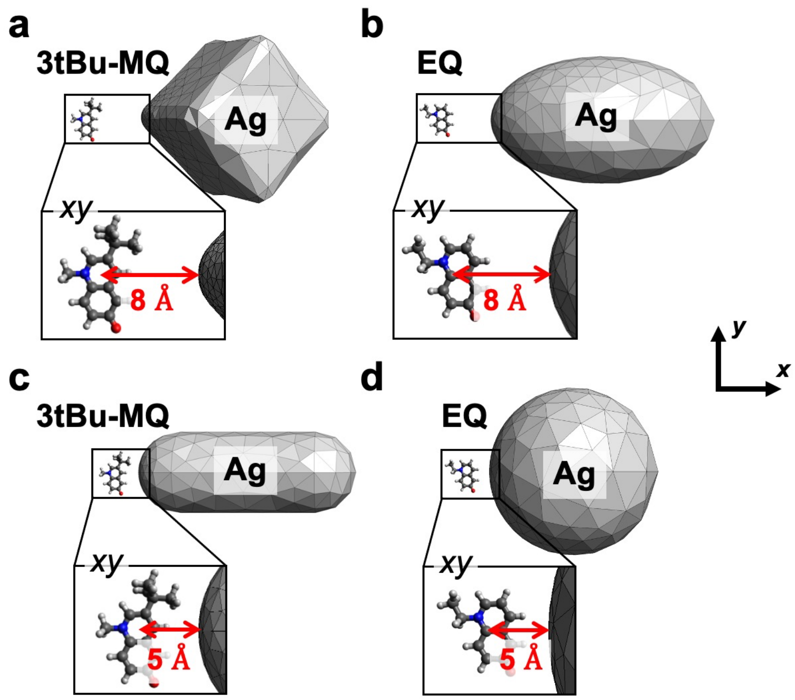

Figure S7. Schematic representations of the designed molecule + metal NP systems obtained in the design of both the molecule and incident electric field. The design was performed on the silver NPs with (a) cubic, (b) ellipsoidal, (c) rod, and (d) spherical shapes. Drawing out of scale.

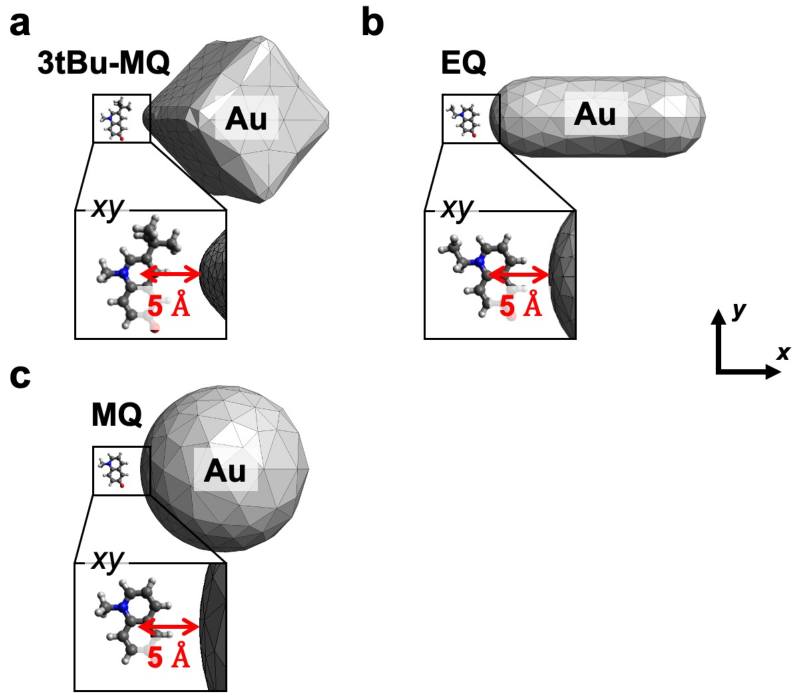

Figure S8. Schematic representations of the designed molecule + metal NP systems obtained in the design of both the molecule and incident electric field. The design was performed on the gold NPs with (a) cubic, (b) rod, and (c) spherical shapes. Drawing out of scale.

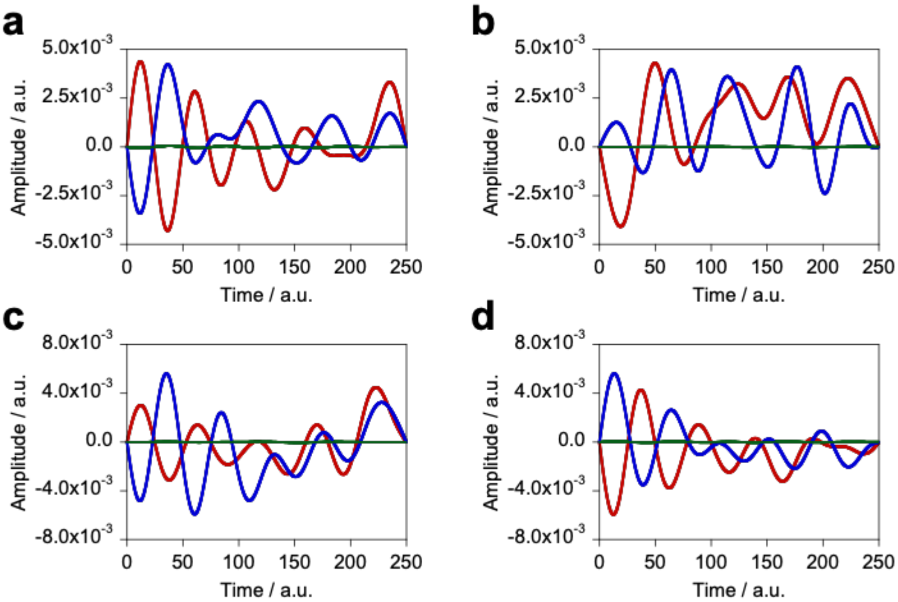

Figure S9. Time profiles of the optimal incident fields obtained in the design of both the molecule and incident electric field. The design was performed on the silver NPs with (a) cubic, (b) ellipsoidal, (c) rod, and (d) spherical shapes. The red, blue, and green lines are the x, y, and z components, respectively.

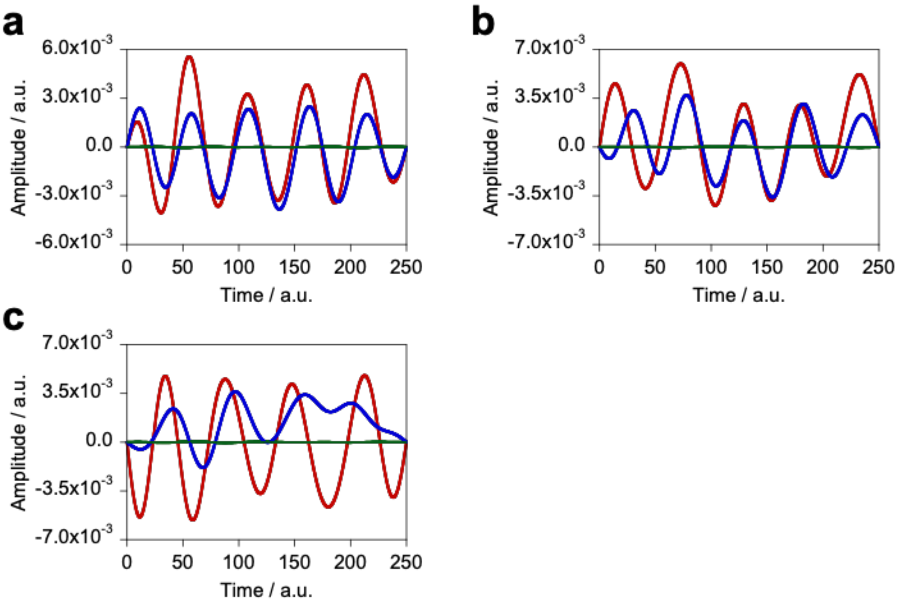

Figure S10. Time profiles of the optimal incident fields obtained in the design of both the molecule and incident electric field. The design was performed on the gold NPs with (a) cubic, (b) rod, and (c) spherical shapes. The red, blue, and green lines are the *x*, *y*, and *z* components, respectively.

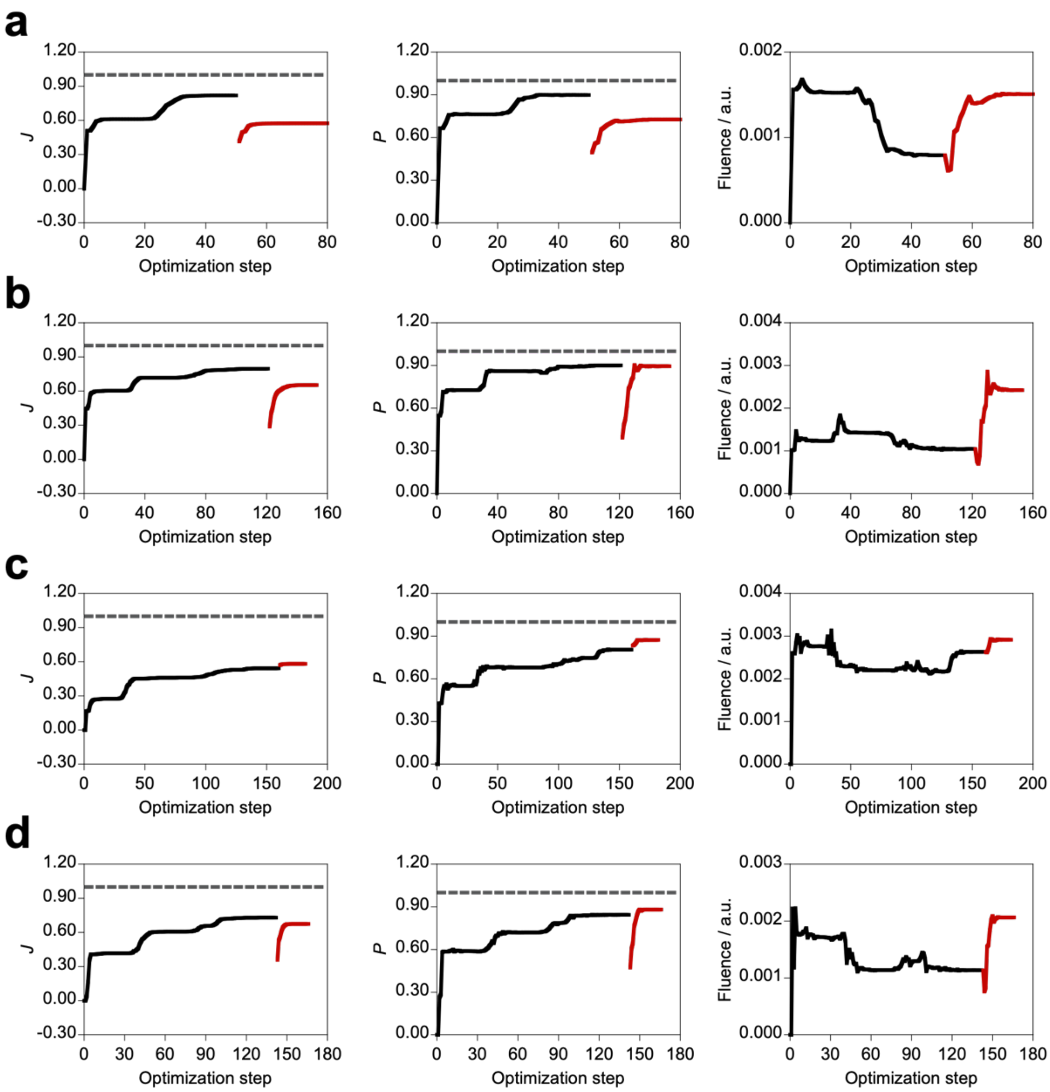

Figure S11. Optimization histories of the objective function in both the optimal molecule and incident field design, along with variations of population of the target state and total fluence of the incident field. The design was performed on the silver NPs with (a) cubic, (b) ellipsoidal, (c) rod, and (d) spherical shapes. The red lines are of the design of the optimal incident field for the optimal molecule. The gray dashed lines denote the value of 1.00.

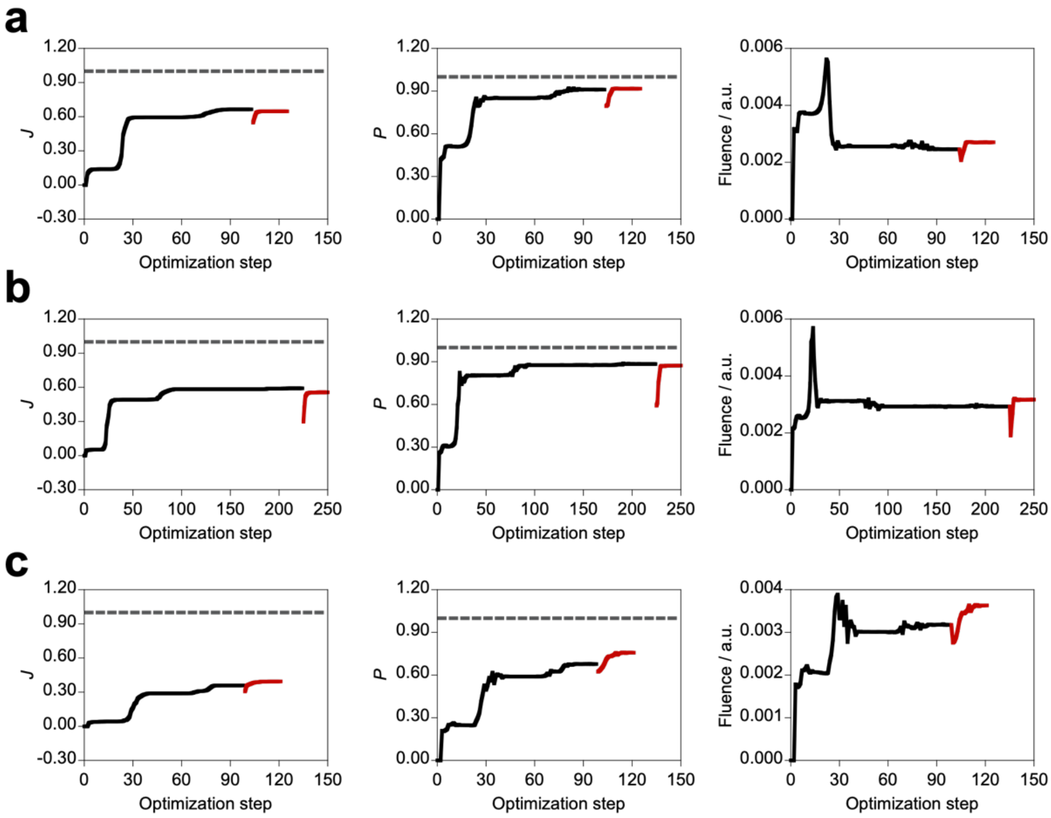

Figure S12. Optimization histories of the objective function in both the optimal molecule and incident field design, along with variations of population of the target state and total fluence of the incident field. The design was performed on the gold NPs with (a) cubic, (b) rod, and (c) spherical shapes. The red lines are of the design of the optimal incident field for the optimal molecule. The gray dashed lines denote the value of 1.00.

A method for designing metal natures of nanoparticles

We also developed a method for designing metal natures of nanoparticles (NPs). Although the proposed method is not computationally effective, it may be useful for combining with constraint conditions that need to be accounted for in the design of realistic materials. Here, details of the design method and the results applied to the present system are given.

The method for designing metal natures of NPs was developed based on the PCM-NP description of metal NPs.[1] Ref. 1 introduces $f(\omega)$ that collects all dependencies on metal natures of NPs in the PCM-NP for developing TD-PCM-NP. A set of polarization charges of metal NPs in the frequency domain has $f(\omega)$ as these coefficients. $f(\omega)$ is written as

$$f(\omega) \approx \sum_p \frac{A_p}{\omega_p^2 - \omega - i\gamma_p \omega}$$

where A_p, ω_p, and γ_p are parameters for a pole denoted by subscript *p*. Because of the additivity of $f(\omega)$ in terms of the poles in this equation, $f(\omega)$ can be decomposed into each contribution of the poles as

$$f(\omega) \approx \sum_p f_p(\omega)$$

where

$$f_p(\omega) = \frac{A_p}{\omega_p^2 - \omega - i\gamma_p \omega}.$$

To design metal natures of NPs, we express $f_p(\omega)$ as a linear combination of the corresponding $f_p(\omega)$ of candidate metal natures, $\{f_{p,k}\}$;

$$f_p(\omega) = \sum_k a_k f_{p,k}(\omega) = \sum_k a_k \frac{A_{p,k}}{\omega_{p,k}^2 - \omega - i\gamma_{p,k}\omega}$$

where a_k is a participation coefficient (weight) for the *k*th candidate metal nature with constraints

$$\sum_k a_k = 1$$
$$0 \le a_k \le 1,\ k = 1,\ 2,\ \cdots$$

As the result, we obtain

$$f(\omega) = \sum_p \sum_k a_k f_{p,k}(\omega) = \sum_p \sum_k a_k \frac{A_{p,k}}{\omega_{p,k}^2 - \omega - i\gamma_{p,k}\omega}.$$

The participation coefficients for the metal natures, $\{a_k\}$, can be optimized to tailor the metal nature of NPs in the design. However, the obtained expression of $f(\omega)$ suggests that the PCM-NP simulation needs to involve all the candidate poles. This demands a large computational cost, resulting in the ineffective design.

We applied the design method to the design of the metal nature of a NP of a molecule–nanocube system. The adopted molecule–nanocube system is shown in Figure S13. The adopted molecule is MQ. For candidate metal natures, we adopted Ag, Al, Au, Cu, Pd, and Rh. We used six poles for all the metals. The experimental data of dielectric functions of the bulk metals were taken from Ref. 2 for Al, Ref. 3 for Cu, Ref. 4 for Pd, and Ref. 5 for Rh. The incident electric field is the Gaussian sinusoidal pulse (equation (17) and Figure 3). The distance between the molecule and the NP surface was set to 5 Å.

The molecular plane of MQ is in the *xy* conformation. The design was performed to maximize the population of the first excited state of MQ at the end of the incident field illumination. The optimization was performed with the same procedure as the inverse design described in the main text.

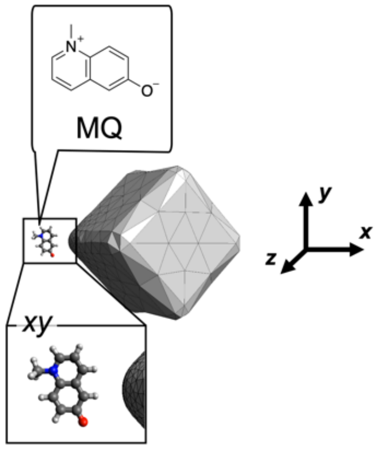

Figure S13. Schematic representation of the MQ molecule + metal nanocube system. *xy* indicates that the molecular plane of MQ is located on the *xy* plane of the Cartesian coordinate. Drawing out of scale.

We tested the design of the metal nature of the NP of the MQ + nanocube system using five different conditions of the randomized initial participation coefficients. It was shown that the Ag nanocube gives the largest population (Table S2). In all the trials, Ag was successfully designed for the metal nature of the NP, one of which is shown in Figure S14. We further analyzed the calculation results. Figure S15 shows imaginary parts of the polarizabilities of the Ag, Al, Au, Cu, Pd, and Rh nanocubes, and these spectra are compared in Figure S16. The plasmonic peak of the Ag nanocube locates near the excitation energy for the first excited state of MQ close to the NP (ca. 3.15 eV), and the polarizability of the Ag NP is larger than those of the NPs with the other metal natures at that frequency. This indicates that the local field generated on the Ag nanocube surface due to the incident field is resonant with molecular excitation energy and therefore contributes to the large population of the target state of the molecule.

Table S2. Screening results for all the metal natures of the NP of the MQ + nanocube system

Metal nature	Population
Ag	1.32×10^{-7}
Al	3.16×10^{-8}
Au	1.73×10^{-8}
Cu	2.52×10^{-8}
Pd	3.01×10^{-8}
Rh	2.91×10^{-8}

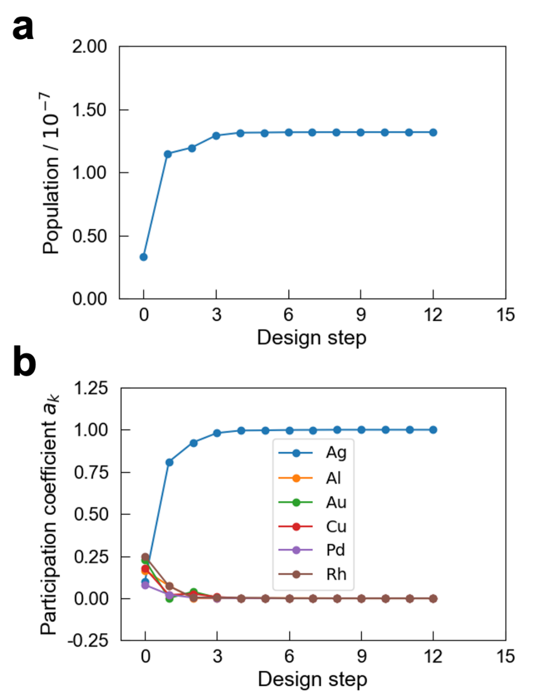

Figure S14. Results of the design of the metal nature of the NP of the MQ + nanocube system. Changes of (a) population of the first excited state of MQ and (b) normalized participation coefficients in the design.

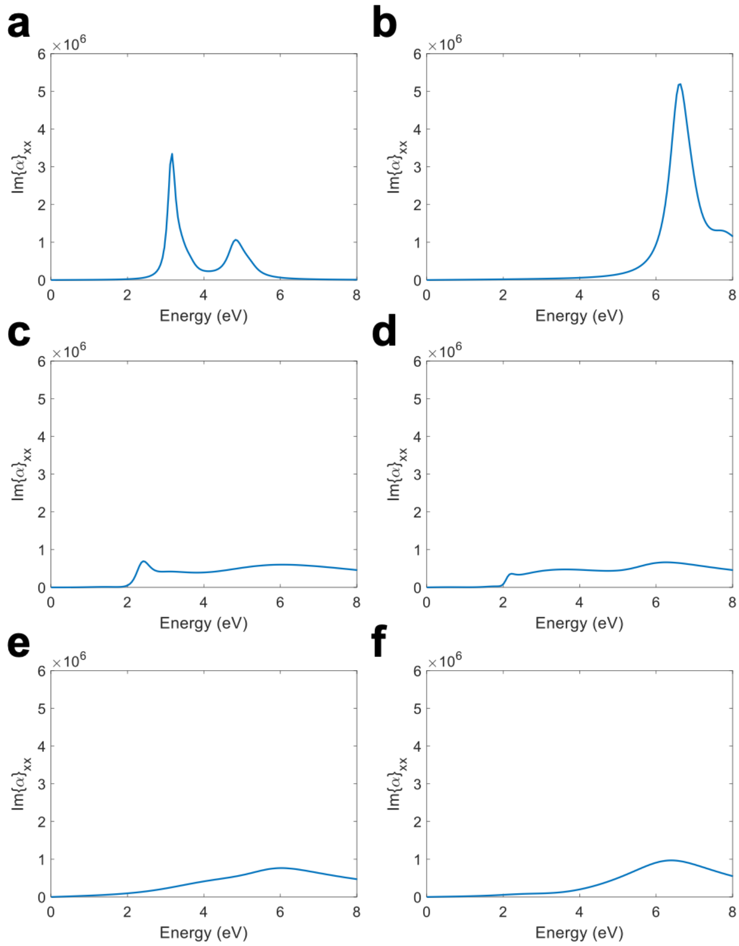

Figure S15. Imaginary part of the polarizability of the (a) Ag, (b) Al, (c) Au, (d) Cu, (e) Pd, and (f) Rh nanocubes.

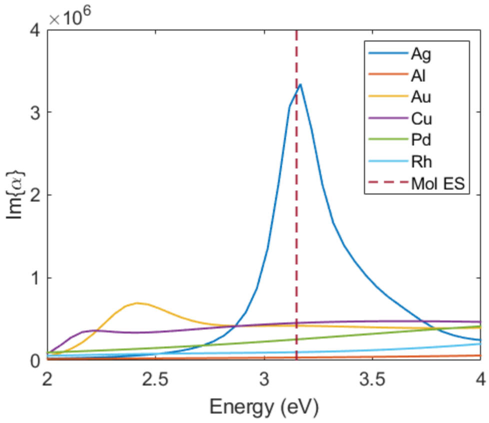

Figure S16. Imaginary parts of the polarizabilities of the Ag, Al, Au, Cu, Pd, and Rh nanocubes and excitation energy for the first excited state of the MQ molecule near the NP (Mol ES).

References

1. G. Dall'Osto, G. Gil, S. Pipolo and S. Corni, *J. Chem. Phys.*, 2020, **153**, 184114.

2. K. M. McPeak, S. V. Jayanti, S. J. Kress, S. Meyer, S. Iotti, A. Rossinelli, D. J. Norris, *ACS Photonics*, 2015, **2**, 326–333.

3. P. B. Johnson, R. W. Christy, *Phys. Rev. B*, 1972, **6**, 4370–4379.

4. P. B. Johnson, R. W. Christy, *Phys. Rev. B*, 1974, **9**, 5056–5070.

5. E. Palik, Handbook of Optical Constants of Solids, Academic Press: Cambridge, MA, USA, 1998.